This document is the accepted manuscript version of the following article:
Guo, H., Luković, M., Mendoza, M., Schlepütz, C. M., Griffa, M., Xu, B., … Burgert, I. (2019). Bioinspired struvite mineralization for fire-resistant wood. ACS Applied Materials and Interfaces, 11(5), 5427-5434. https://doi.org/10.1021/acsami.8b19967

Bioinspired struvite mineralization for fire resistant wood

Huizhang Guo[1,2*], Mirko Luković[3], Miller Mendoza[3], Christian M. Schlepütz[4], Michele Griffa[5], Biwan Xu[5], Sabyasachi Gaan[6], Hans Herrmann[3] and Ingo Burgert[1,2*]

[1]Wood Materials Science, Institute for Building Materials, ETH Zürich, 8093 Zürich, Switzerland.

[2]Applied Wood Materials, Empa-Swiss Federal Laboratories for Materials Science and Technology, 8600 Dübendorf, Switzerland.

[3]Comuptational Physics for Engineering Materials, Institute for Building Materials, ETH Zürich, 8093 Zürich, Switzerland.

[4]Swiss Light Source, Paul Scherrer Institute, 5232 Villigen, Switzerland.

[5]Concrete/Construction Chemistry, Empa-Swiss Federal Laboratories for Materials Science and Technology, 8600 Dübendorf, Switzerland.

[6]Advanced Fibers, Empa-Swiss Federal Laboratories for Materials Science and Technology, 9014 St. Gallen, Switzerland.

*Corresponding Author: huguo@ethz.ch; iburgert@ethz.ch.

Keywords: Fire resistant wood, Mineralization, Struvite mineral, X-ray tomography, Lattice Boltzmann.

ABSTRACT

High-performance wood materials have attracted significant attention in recent years due to excellent property profiles achieved by relatively easy top-down processing of a renewable resource. A crucial flaw of the renewable wood scaffolds is the low flame retardancy, which we tackled by bio-inspired mineralization in an eco-friendly processing step. The formation of the biomineral struvite, commonly found in urinary tract stones, was used for the infiltration of hierarchical wood structures with the necessary ions followed by an in-situ synthesis of struvite by ammonium steam fumigation. Struvite

decomposes prior to wood, which absorbs heat and releases non-flammable gas and amorphous $MgHPO_4$ resulting from the degradation promotes insulating char formation. As a result, the mineralized wood can hardly be ignited and the treatment strongly suppresses heat release rate and smoke production.

INTRODUCTION

Modification and functionalization of the hierarchical structure of wood in easy scalable top-down approaches result in high-performance wood materials. By preserving the integrity and fiber directionality of the cellulose scaffold, exceptional mechanical properties have been achieved[1-2] or new functions such as transparency[3-6] or magnetic ability[7] can been implemented. A severe obstacle for enhanced utilization of these renewable and CO_2 storing materials and substitution of less eco-friendly materials is the inherent flammability of wood, which has led to severe fire catastrophes in history and has been engraved in people`s awareness.

Fire protection treatments of wood by conventionally used flame-retardants often possess halogenated compounds, which can cause environmental and health issues.[8-9] An eco-friendly alternative is based on nanostructured clay minerals,[10] such as fire retardant paper consisting of cellulose nanofibers and clay nanoplates.[11-12] Recent studies also showed that the addition of graphenoids could significantly improve fire retardancy of organic-inorganic composites,[13-14] which includes nanocomposites of graphene oxide and montmorillonite clay nanosheets.[15] However, most of today`s fire retardant organic-inorganic composites are fabricated through a bottom-up process,[15] which limits their application to large-scale bulk materials such as wood and hence, the fabrication of non-toxic flame-retardant materials for larger scale application is still a major challenge.[16]

Biomineralization by living organisms leads to advanced inorganic/organic hybrid materials under ambient conditions, including the formation of silicates, carbonates and calcium phosphates in soft tissues.[17-19] The underlying mechanisms and the achieved property profiles of seashells or bone have been studied in great detail, in particular as biological role models for the development of strong and tough materials.[20] Inspired by nature`s matrix-mediated biomineralization, Merk et al. mineralized wood with

$CaCO_3$.[21-22] The resulting wood-inorganic hybrid materials showed significantly reduced heat release rates and smoke production. However, $CaCO_3$ decomposes at a higher temperature than wood, impeding a major impact of the treatment on ignition inhibition.

Struvite ($MgNH_4PO_4 \cdot 6H_2O$) is a phosphate biomineral, which is commonly found in urinary tract stones of dogs, cats, and humans. The formation is caused by a bacterial infection that hydrolyzes urea to ammonium and raises urine pH to be neutral or alkaline.[23] This mineralization process, which takes place under mild conditions, is a source of bio-inspiration for the formation of wood-mineral hybrid materials with improved flame retardancy. Struvite recovered from synthetic wastewater was used as a fire-retardant barrier for both cotton fabric and wooden plates.[24] Hanagasaki injected wood with an acid solution, which contained fire retardants including phosphate, magnesium and ammonium compounds. Then the wood was brought in contact with an alkaline aqueous solution to form a poor solubility substance for fire-retardancy.[25] In the event of a fire, the endothermic decomposition of struvite occurs prior to the decomposition of wood and releases non-flammable gases to dilute the flammable gases in the wood structure. Furthermore, it forms amorphous $MgHPO_4$ in the degradation process that acts as a gas barrier and catalyzes the cross-linking of the wood-polymer, resulting in a significant increase in insulating char formation.[26]

RESULTS AND DISCUSSION

We infiltrated the porous wood structure with a potassium and magnesium salt solution by vacuum impregnation **(**Figure 1a**)**. Ammonium fumigation was used to potentiate the mineralization, in which ammonia is a reactant resulting in struvite mineral also adjusting an alkaline pH of the salt solution to achieve struvite precipitation (Equation S1 and S2).[27] The distribution of the minerals in struvite-wood was studied by SEM combined with EDS. The EDS spectrum displays the carbon in the wood, along with peaks assigned to Mg and P, which originate from the struvite mineral embedded in the wood structure (Figure 1b). The weak signals associated with S and K stem from the soluble compounds (such as K_2SO_4) that were not entirely removed by the leaching treatment. Both the Mg and the P are located in the lumen

as well as in the middle lamella, indicating the struvite mineral distribution pattern (Figure S1 in the Supplementary Information). The XRD pattern of struvite-wood shows blended crystal phases (Figure 1c and Figure S2). Two broad peaks at 18º and 26º relate to the crystalline cellulose in wood. The majority of the diffraction peaks are attributed to the struvite mineral. Some small angle diffraction peaks are also observed that signify the presence of newberyite minerals ($MgHPO_4 \cdot 3H_2O$).

Synchrotron X-ray tomographic microscopy in conjunction with propagation-based phase contrast enhancement was used to visualize and study the three-dimensional structure of the mineralized wood. Mutually orthogonal planar cross-sections from the reconstructed three-dimensional volume (tomogram) (Figure 1d, Figure S3 and Movie S1) display the porous structure of wood, in which tracheids, as the main structural elements of softwood, are orientated in parallel to the longitudinal direction of the stem with a length of around 3 millimeters, a diameter of ~10 to ~40 µm and a cell wall thickness of ~2 to ~10 µm. The cell lumina of the tracheids are empty macropores. Rays, consisting mainly of parenchyma cells run in the radial direction of the stem. The contrast enhancement achieved by phase contrast reconstruction allows for a automatic classification (by 3D image analysis, see the Supplementary Information) and visualization of the mineral distribution in the wood structure and shows that the minerals accumulate mainly in the cell lumina of tracheids and the ray parenchyma (Figure 1e and Figure S4, Movie S2). The embedded minerals have a volume fraction of about 22% (total struvite volume divided by total specimen volume) and a lumen filling ratio of about 46% (ratio of struvite volume and pore space volume). To demonstrate the mineralization depth, we mineralized a wooden block with a dimension of 100 mm × 20 mm × 20 mm in longitudinal × radial × tangential direction, resulting in a mass gain of 95 %. SEM images acquired from the center of the sample indicate that minerals were formed in the whole sample (Figure S5).

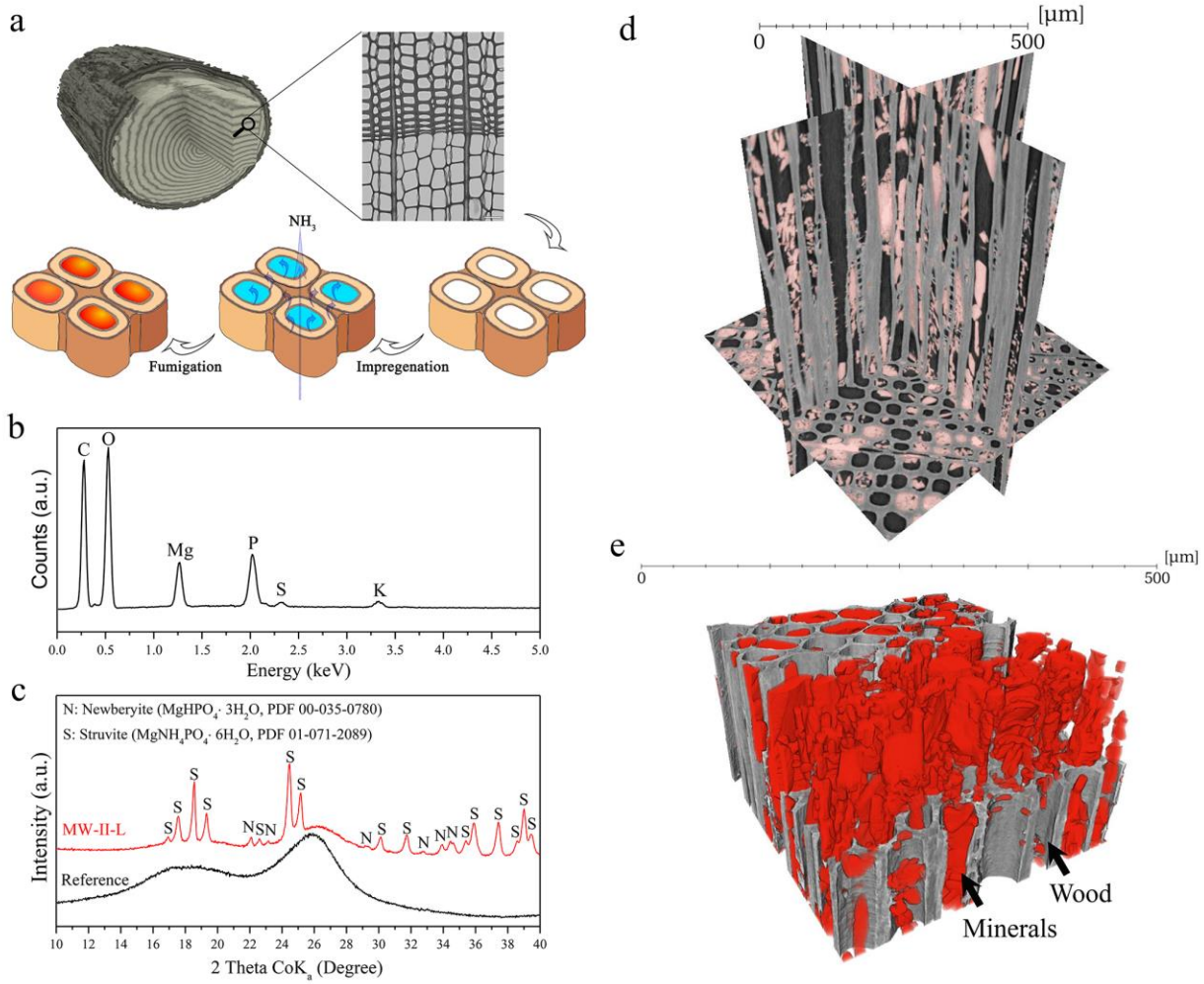

Figure. 1. The schematic illustration of the bio-inspired mineralization of wood and structural characterization. (a) the mineralization process includes a vacuum impregnation of the precursor solution into the pores of wood followed by ammonium hydroxide fumigation. (b) EDX spectrum of struvite-wood. (c) XRD patterns of native wood and struvite-wood. (d) three-dimensional rendering of three planar, mutually orthogonal, cross-sections of the X-ray tomogram; one cross-section is orthogonal to the longitudinal direction of the wood structure; darker voxel value means smaller electron density; the voxels rendered in semi-transparent red are those classified as belonging to the struvite particles. (e) Three-Dimensional rendering of a small region-of-interest (ROI) from the analyzed X-ray tomogram, with voxels assigned to struvite particles rendered in red, while the wood cell wall is rendered in almost fully opaque grey tones. In (e), part of the rendered cell wall is removed (front side) for better visualization of the struvite voxels rendered in red.

To assess the fire-retardant properties of struvite-wood panels in a simulated fire event, we investigated the heat release rate (HRR) and dynamic smoke production rate (SPR) by cone calorimetry measurements. The natural wood panels display a typical HRR curve of thermally thick charring materials (Figure 2a), which showed an HRR peak immediately after ignition, before charring.[28] The second major HRR peak appeared after 405 seconds most probably due to cracking of the char layer. The struvite-wood also exhibited two HRR peaks, which were significantly lower and delayed for the second peak. The visual observation during the cone calorimeter test showed an intensive fire spread of the natural spruce after 405 seconds (Figure 2e and Movie S3), while there was only a weak fire spread observed for struvite-wood (Figure 2f and Movie S4). The total heat release (THR) for struvite-wood was only 65% of the natural wood, 47.35 MJ/m^2 versus 72.10 MJ/m^2, respectively (Figure 2b). Furthermore, CO production and smoke release are critical parameters in a fire hazard. The smoke release rate (SRR) of the natural spruce wood coincides well with the heat release during the cone calorimeter test (Figure 2c). The first SRR peak appears immediately after the ignition. The low SRR from 100 s to 300 s indicates the forming of a char layer that suppresses further decomposition. The second SRR peak appeared upon cracking of the char layer, causing a rapid heat penetration and further decomposition of wood. Struvite-wood exhibited strongly reduced SRR peaks, and the total smoke release (TSR) was highly suppressed compared to natural spruce wood (Figure 2d).

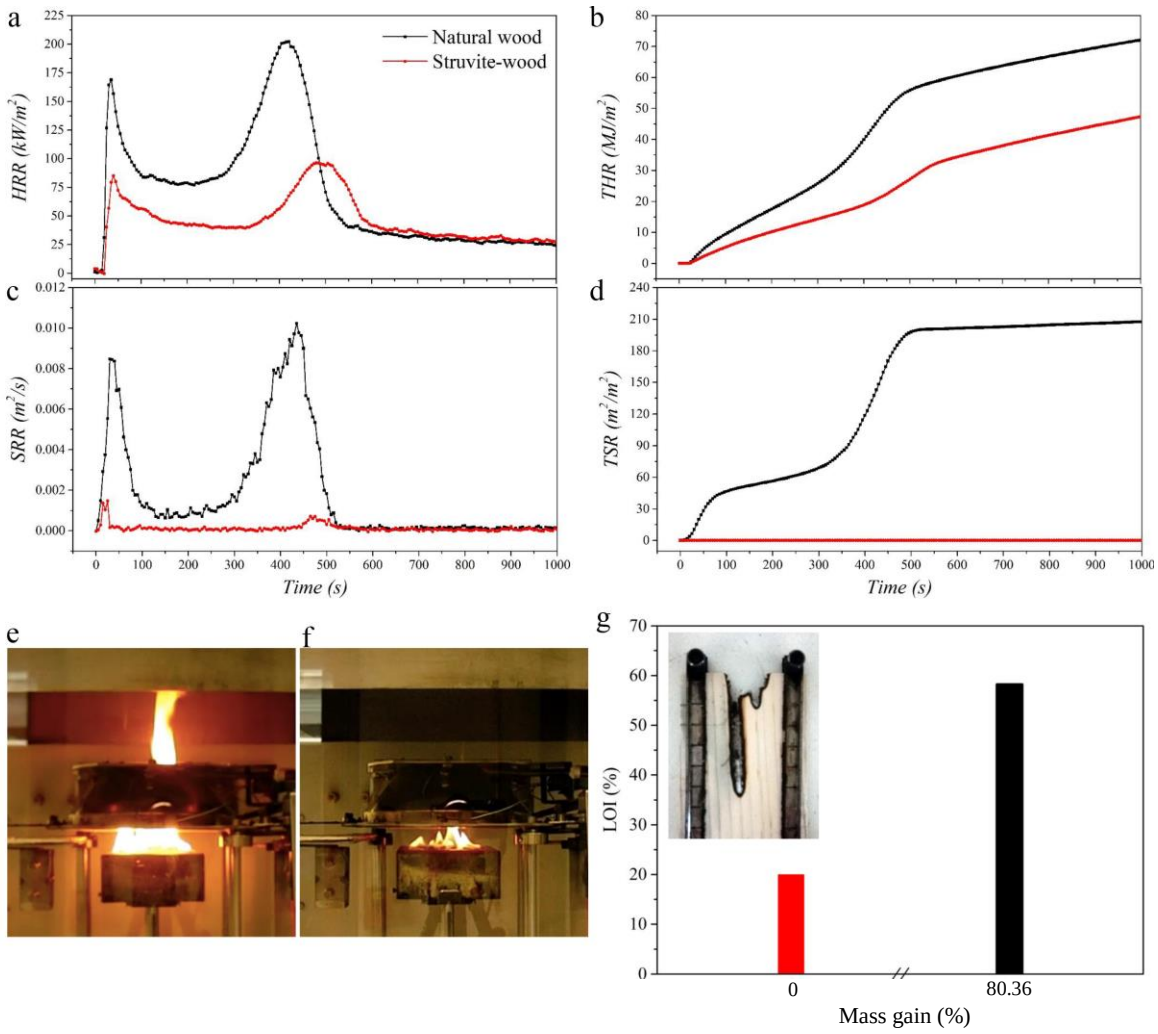

Figure 2. Cone calorimeter measurement. (a) the average heat release rate (HR4R). (b) total heat release (THR). (c) smoke release rate (SRR). (d) total smoke release (TSR). (e) and (f) images of the natural wood and struvite-wood taken after 405 seconds during the colorimeter run. (g) LOI values of natural wood (black) and struvite-wood (red); the inset displays the struvite-wood after LOI measurement.

To access the ignitability of struvite-wood, we subjected thin wood veneers to a direct flame with a single-flame source. The natural wood veneer was ignited in two seconds after direct exposure to the flame and burning intensively to ash in ~ 40 seconds **(**Movie S5**)**. Struvite-wood was resistant to direct flame exposure and could not be ignited during two consecutive attempts of 10 seconds each time (Movie S6 and Figure S6). Limited oxygen index (LOI) measurements according to the ASTM D2863 standard determined the minimum oxygen concentration that can sustain flaming after removal of an ignition

source. The struvite-wood with a mass gain of 80.36 % was hardly ignited in a normal atmosphere, as the LOI of struvite-wood was measured to be 58.25 %, which is about three times higher than that of the natural spruce wood (Figure 2g). The mineral contents and respective LOIs are strongly depending on the mineralization protocol. Preceding studies with only one mineralization step and subequent water leaching of remaining soluble compounds showed that the content of minerals in wood (mass gain) as well as the leaching treatment have strong effect on the fire resistance of the mineralized wood. The one-time mineralization (MW-I) resulted in an average weight gain of 73.65 % and a LOI of 58.75 %. The subsequent leaching step reduced the average weight gain to 42.89 % and a LOI of 37.00 % (MW-I-L) (supporting information, Table S1).

To unravel the basic mechanism of the fire-retardant effect of struvite-wood, we performed experiments and computer simulation of the decomposition behavior of struvite-wood. The natural wood and a freestanding struvite powder were analyzed by thermogravimetric analysis (TGA) and differential scanning calorimetry (DSC). The natural wood showed an initial weight loss because of the vaporization of adsorbed water below 100 ˚C with a derivative weight peak at 50 ˚C, then followed by the decomposition of organic wood compounds in three main different temperature ranges (Figure 3).[29-30] The struvite minerals mainly decomposed before 180 ˚C with two peaks located at ~115 ˚C and ~143 ˚C via an endothermic reaction (**Figure S7**). The DTA curve of struvite-wood demonstrates that the mineralized wood has an additional decomposition peak prior to wood degradation. As a result, the separated degradation peaks belonging to hemicellulose and cellulose, which were observed in the DTA curve of native wood, were suppressed. The inert gases released during the reaction diluted oxygen and the flammable gases in the flame. The endothermic reaction, together with the release of inflammable gases explains self-extinction after the removal of an external fire source as shown in the single flame test experiment. The struvite mineral decomposition in the TGA experiment resulted in a mass loss of around 50 % at the end of the heating process, which is close to a calculated theoretical value according to Equation S3 and S4. It revealed that the struvite mineral is completely converted into $MgHPO_4$ which

contains an acidic OH that may catalyze the char formation of the organic compounds of wood.[31-32, 33] This explains the enhanced char formation due to the interactions of $MgHPO_4$ with organic wood compounds serving as an insulating fire barrier that prevents the inner wood of a timber element from burning and could also contribute to reduced smoke generation (Figure 2).

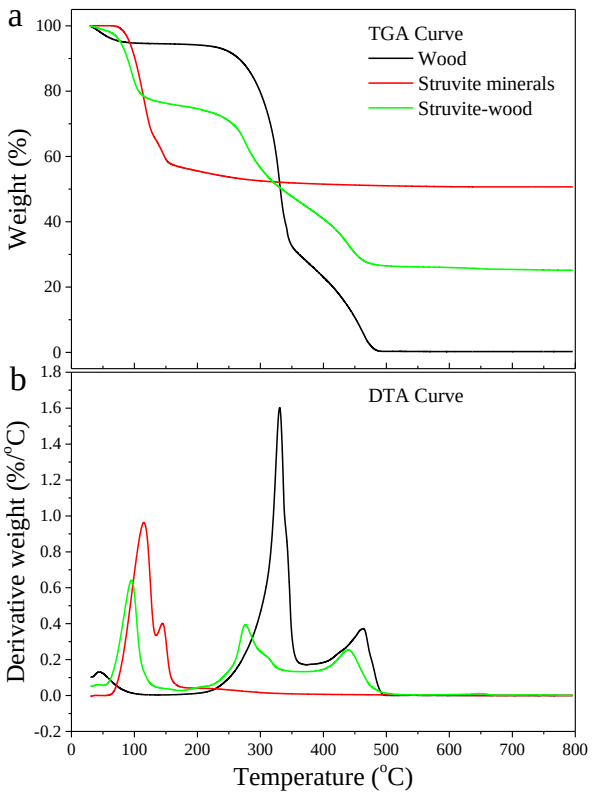

Figure 3. Thermal analysis. (a) The mass loss of the sample components while subjected to a temperature gradient up to 800 ˚C at a heating rate of 10 ˚C ·min^{-1} with the air purge. (b) The first derivative of the TGA curve (the DTG curve) was further plotted for an in-depth interpretation of the decomposition of the mineralized wood.

The charring process was further analyzed by combustion of small specimens of struvite-wood and natural wood at 600 ˚C in an oven for 10 min. Struvite-wood turned into a carbon layer with a mass loss of ~66.2 %, while the reference was burned to ash with a mass loss of 99.71% (Figure 4a). The cell wall of the struvite-wood became highly porous after combustion with the decomposed mineral particles

embedded (Mg and P) inside the remaining cell walls as well as attached to the lumen surface (Figure 4b-d). Carbon was mainly located in the remaining cell walls resulting from the pyrolysis or oxidative decomposition during the heat treatment at 600 ˚C (Figure 4e-i). The penetration of the mineral compounds into the wood cell wall was further confirmed by STEM-EDS analysis (Figure S8 and S9).

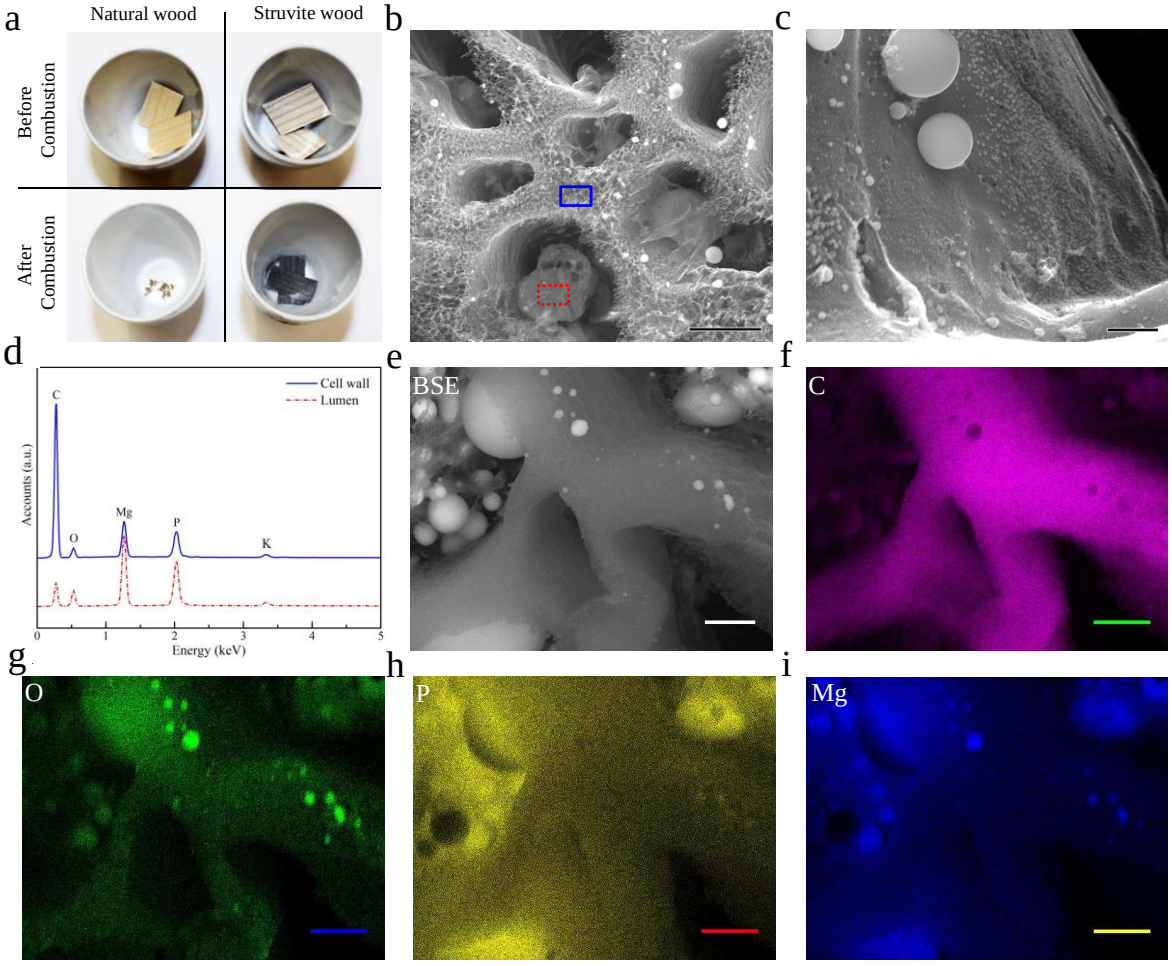

Figure 4. The structural and compositional characterization of the wood char. (a) Photograph of struvite-wood and native wood before and after heat treatment at 600 ˚C for 10 min. (b) SEM image of the transverse section of the charred wood. (c) SEM image of the lumen surface of the charred wood. (d) EDX spectra acquired from the cell wall (blue) and the lumen (red) of the charred wood. (e) to (i) BSE SEM images mapped by element. The scale bar is 20 µm in (b), 2 µm in (c), and 5 µm in (e) to (i).

In a complimentary computer simulation of heat transport in the specimen, we studied the heat absorption effect of the mineral during decomposition and the suppression of the combustion and generation of char by the amorphous $MgHPO_4$ resulting from the demineralization in the flame zone (Figure 5). We used the Lattice Boltzmann model to solve the heat equation (described in detail in SI),[34] which has been proven to be an accurate and efficient tool for handling complex geometries, such as wood structures (Figure S10).[35] The evolution of temperature was simulated with the heat equation (Eq. 1) on cross-sections of the sample shown in Figs. 5a and 5d.

$$\frac{\partial T}{\partial t} = \alpha \nabla^2 T \qquad \text{(Eq. 1)}$$

In Eq. 1, T is the local temperature of the sample and α the local thermal diffusivity. We discretized the struvite-wood into voxels. For the discretization, each voxel only contains one single material type, which can either be the cell wall of wood (brown), the air inside the lumen (white), the struvite deposited inside the wood lumen (purple), the glassy newberyite (blue), or the char (black). The dimension of the sample is 1728 × 1820 voxels where each voxel has a linear dimension of 325 nm.

The model allows simulating the material transformation caused by heating in natural and struvite-wood. It shows that one-sided heating to 600°C results in enhanced char formation in the mineralized wood with porous cell-like structures (Figure 5b and Movie S7). Based on the simulation results, the wall thickness of the char was estimated to be 3 µm, which is in a good agreement with the average thickness of the charred structures measured from tomography images acquired from the struvite-wood after heat treatment in a 600 ˚C heated oven for 10 min (Figure S11 and Figure S12). The char layers are formed because of the presence of the struvite mineral in the wood, and their formation plays the most important role in slowing down the heat transfer across the sample (Figure 5c). The natural wood does not show any char formation and decomposes completely to ash (Figure 5e and Movie S8). As a result, the fire can advance quickly without the char layer as a barrier (Figure 5f). In the event of a fire, one typically observes char formation in natural wooden beams and shells used in construction. However, the heat

distribution is different from the simulated case, in which a very small wood section is directly exposed to a heat source of 600°C. A gradual increase in temperature results in more char production than a sharp increase, because the char production is dependent on low-temperature dehydration reactions.[26] By comparing the simulation of heat transfer in natural wood with that in mineralized wood, we conclude that the addition of struvite strongly slows down the heating process by a factor of about 85.

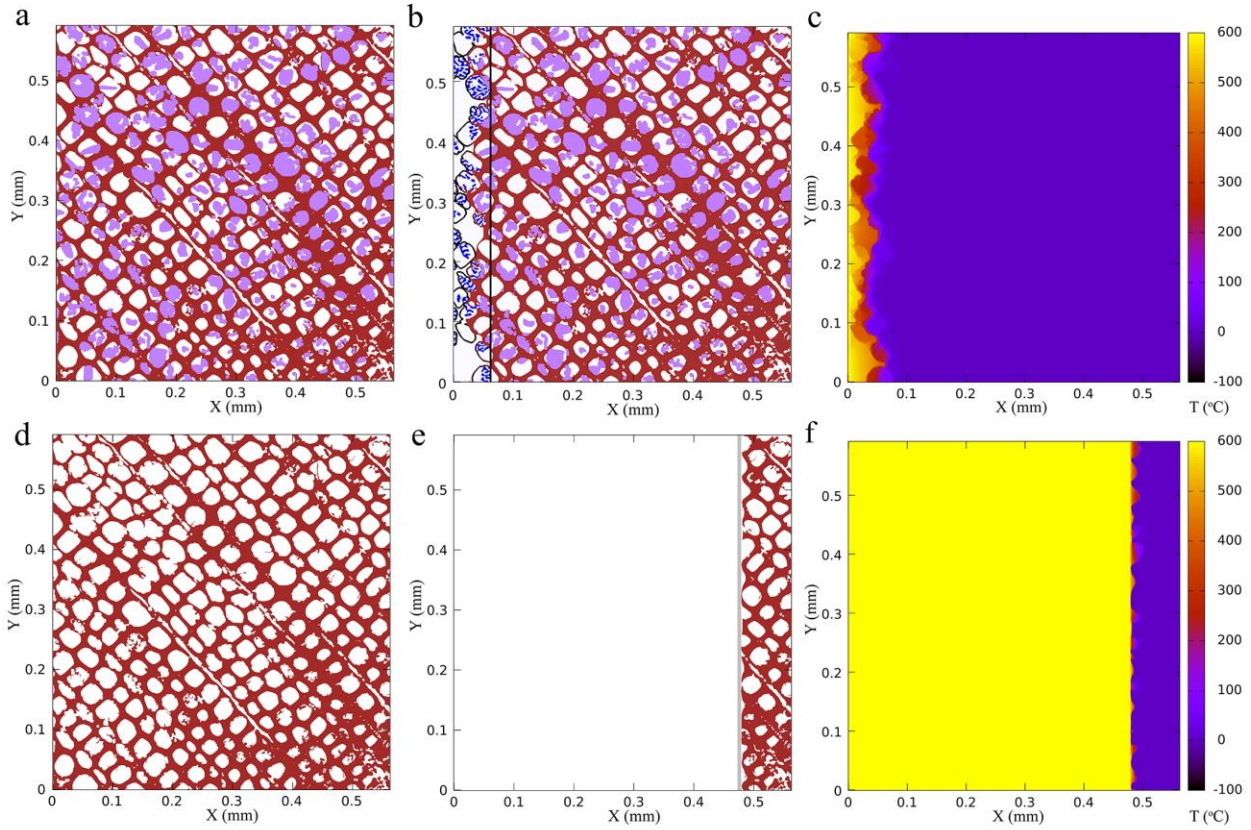

Figure 5. Material structure and temperature of the simulation sample. (a) The initial geometry of the struvite-wood, which is constructed from the tomography images of struvite-wood. (b) The material composition of struvite-wood after 35,000 steps of the simulation. The vertical black line indicates the furthest extent of char formation at 0.06 mm. (c) The temperature distribution of struvite-wood after 35,000 steps of the simulation. The heat source is placed along the y-axis at x=0 and is kept at a constant temperature of 600 ˚C. (d) The initial geometry of the natural wood after taking the mineral phase away from (a). (e) The composition of wood after 35,000 steps of the simulation. The vertical grey line is the

moving heat source boundary, kept at a constant temperature of 600 °C. (f) The temperature distribution of wood after 35,000 simulation steps. In (a), (b), (d) and (e), red represents the wood cell wall, purple the struvite mineral, white air inside the lumen, blue the amorphous $MgHPO_4$, and black the char.

CONCLUSIONS

The flame retardancy of wood can be strongly improved by bio-inspired struvite mineralization in an easily scalable top-down process. The mineralization process results in a good mineral particle penetration depth to provide fire-retardant properties. The ammonia fumigation initiates the growth of struvite mineral without a direct contact of wood with alkaline solution and the excessive ammonia is removed during the drying process. The mineral formation inside the wood structure enables a bulk treatment in contrast to directly using struvite mineral as a barrier layer. The interplay of the mineral phase and the wood scaffold at the nano- and microscale allows for an improved flame retardancy while retaining the natural appearance of wood. Both experiment and modeling show that the main factor governing the fire retarding capacity of wood is the carbonaceous char formation, which is facilitated by the embedding of struvite in the bulk wood structure. The char forms an insulating layer that is responsible for the retardation of oxygen diffusion, heat insulation and the reduction of the volatilization of flammable gas. The increased char formation of the mineralized wood can be explained by two complementing factors. The endothermic decomposition and the emission of non-flammable gases prevent a sharp temperature increase and facilitate char formation. Furthermore, the decomposed mineral ($MgHPO_4$) acts as a catalyst that promotes the devolatilization reaction of cellulose, particularly at low temperatures and results in a cross-linking to a three-dimensional structure, preventing further devolatilization. Most probably, this is due to the formation of acidic phosphate during the decomposition of the struvite mineral, which absorbs heat, releases non-flammable gases and strongly enhances the char formation as a cross-linker. The increased char layer of struvite-wood is highly beneficial for wood applications as it can serve as an insulation barrier delaying the burning process in the event of a fire. The simple and green top-down process will have a strong impact on the utilization of high-performance wood

materials in various fields of application, promoting the essential substitution of less eco-friendly materials.

MATERIALS AND METHODS

Material: Norway spruce (*Picea abies*) was used as the wood material. Anhydrous magnesium sulfate (199g, MgSO4, ⩾99.5%) was purchased from Sigma; Potassium phosphate monobasic (KH_2PO_4, 99%,) was purchased from Chemie Brunschwig AG; Ammonium hydroxide solution ($NH_4{\cdot}OH$, 25%) was purchased from VWR International AG.

***Preparation of salt solution*:** $MgSO_4$ (199 g) and KH_2PO_4 (225 g) were put into a 2.5 L beaker, then 1.5 L of deionized water was gently poured into the beaker. The solution was vigorously stirred until it turned to clear. Finally, the beaker was sealed by Parafilm and stored until usage.

Mineralization and leaching treatment: In a typical procedure, we used wood veneer with a dimension of 0.8 mm in the radial direction, 50 mm in the tangential direction and 150 mm in the longitudinal direction. The wood samples were stored in a climate room at 65 % relative humidity and 20 ˚C climate until the wood moisture content was constant. Then the weight of the sample (m_1) was measured. Nine wood veneers were placed into a plastic box, which was loaded into a vacuum chamber. The vacuum chamber was pumped down to about 10 mbar and held for 1 hour before the salt solution was sucked into the plastic box until all of the wood veneers were covered. The pressure of the chamber was kept at 10 mbar for another 30 minutes to remove the gas inside the pores of wood further. Then the vacuum was released to ambient pressure and held for 30 mins, by which the salt solution was further pressed into the wood pores. For one mineralization step, the vacuum impregnation process was repeated for three times. Finally, the wood samples were taken out from the vacuum chamber and wiped to remove the excess salt solution from the surface. The salt solution that was impregnated into the wood samples was converted to struvite minerals by ammonium fumigation. The wood samples were placed in a plastic box. A total of 150 mL of ammonium hydroxide solution was added to a glass beaker. The beaker with ammonium hydroxide solution was then loaded into the plastic box mentioned above which was then sealed by a lip.

The “bottle in bottle” setup for fumigation was designed to avoid the direct contact between the ammonium solution and the salt solution impregnated in wood. The ammonium fumigation time was 10 hours. After that, the struvite-wood samples were dried in an oven at 40 °C for 24 hours. A leaching process was used to remove the soluble compounds in the mineralized wood samples. The leaching process was performed by immersing the modified wood veneer into 300 mL of deionized water for 24 hours followed by drying at 40 °C for 24 hours. The same mineralization and leaching processes were repeated once again. The samples were named as struvite-wood. Finally, all of the samples were stored again at 65 % relative humidity and 20 °C until the moisture content was constant.

In preceding studies for an optimization of the mineralization protocol, mineralized wood samples were also produced in only one mineralization step with and without subsequent leaching experiment. The impact on mass gain and fire-retardant properties is stated in the supporting information (Table S1).

Finally, the weight of the modified wood sample (m_2) was measured, and the mass gain (MG) induced by the mineralization was calculated according to the following equation:

$$MG = \frac{m_2 - m_1}{m_1} \qquad \text{(Eq. 2)}$$

Further wood panels with a dimension of 10 mm in the radial direction, 100 mm in tangential and longitudinal direction were used to prepare wood samples for cone calorimeter measurements according to the ISO 5660-1 norm. The leaching treatment was carried out by immersing three pieces of the wood panel into 1 liter of deionized water.

Freestanding struvite mineral was synthesized by exposure of the salt solution to ammonium steam for 10 hours. The precipitate was collected by filtration, followed by washing with deionized water ten times. Finally, the struvite minerals were stored at 65 % relative humidity and 20 °C.

Fire-retardant properties: Limit oxygen index (LOI) (Fire Testing Technology Instrument, East Grinstead, UK) measurements were carried out according to ASTM D2863 to determine the minimum oxygen concentration to support candle-like combustion of the wood veneers. The wood veneer is supported vertically in a mixture of oxygen and nitrogen flowing upwards through a transparent chimney.

The upper end of the specimen is ignited, and the subsequent burning behavior of the specimen is observed to compare the period during which burning continues or the length of the burnt specimen, with specified limits for each burning. The LOI is determined as the minimum oxygen concentration that can keep the wood veneer burning for more than 3 min or longer than a distance of 5 cm. Cone calorimetry (Fire Testing Technology Instrument, East Grinstead, UK) measurements were carried out according to the ISO 5660-1:2002 norm to assess the heat release rate and dynamic smoke production rate for specimens exposed in horizontal orientation to controlled levels of irradiance with an external igniter (conical heater). The igniter provided a constant heat flux of 50 $kW \cdot m^{-2}$ ($T \approx 750^\circ$ C).

Characterization: The freestanding struvite minerals, as well as the mineralized and natural wood, were analyzed by X-ray diffraction (XRD) in Bragg-Brentano mode in $\theta-2\theta$ geometry with Co−Kα radiation (PANalytical, Almelo, The Netherlands). The minerals distribution in the wood pores was analyzed by a scanning electron microscope (SEM, FEI Quanta 200F) with Energy Dispersive X-ray Spectroscopy (EDS). Broad ion beam (BIB) cross sectioning was applied for preparing accurate cross-sectional surfaces in an ion milling systems (Hitachi BIB 4000) for EDS-mapping. Thermal analysis was performed through the use of Differential Scanning Calorimetry (DSC, TA Q2000) and Thermogravimetric Analysis (TGA, TA Q50). For the TGA analysis, about 10 mg of the wood samples were cut into small chips and placed in a platinum pan (100 µL). The conversion of the TGA curve to its derivative mode (DTG) was undertaken from the rate of mass loss curve as a function of temperature. For DSC analysis, about 2 mg of the wood samples were cut into small chips and loaded in a Tzero Aluminum pan. Analyses were performed in a nitrogen or dry air flow of 50 $mL \cdot min^{-1}$. The temperature was ramped from 40 $^\circ$C to 800 $^\circ$C applying a heating rate of 10 $^\circ C \cdot min^{-1}$. The thermal analysis results were processed using Universal Analysis software (TA Instruments). The TEM specimens were prepared by embedding the wood sample in Spurr resin,[36] followed by cutting a transverse section of ~ 150 nm in thickness with a Reicher-Jung Ultracut Ultramicrotome using a diamond knife and mounted on the lacey carbon films on 200 mesh copper grids. High Angle Annular Dark Field-Scanning Transmission electron microscopy (HAADF-

STEM) and Energy Dispersive Spectrometer (EDS) studies were carried out in FEI Talos working with an accelerated voltage of 200 kV.

Please refer to the Supplementary Materials for further details about synchrotron X-ray tomography and modeling of the combustion process.

CONFLICTS OF INTEREST

There are no conflicts to declare.

ACKNOWLEDGMENT: The authors thank Anja Huch for supporting in TEM lamella cutting. The authors also thank Johanna Scoul and Milijana Jovic for their support in fire testing experiments. The authors acknowledge the Paul Scherrer Institut, Villigen, Switzerland for provision of synchrotron radiation beamtime at the TOMCAT beamline X02DA of the SLS. The work was financially supported by Climate-KIC, BTA Urban transition demonstrator project and Innosuisse, Project 28473.1 PFIW-IW. Electronic microscopy analysis was performed in ScopeM at ETH Zürich. Part of the 3D image analysis was performed by the use of the Empa Platform for Image Analysis (https://www.empa.ch/web/s499/software-/-imaging-platform) at Empa's Center for X-ray Analytics.

AUTHOR'S CONTRIBUTIONS: H.G. designed the experiment, carried out mineralization, materials characterization and fire-retardant assessment and wrote the first draft of the manuscript. M.L., M.M., and H.J.H modeled and simulated the heat transport and combustion process and wrote the text related to the modeling and simulation part. C.S. and H.G. performed the Synchrotron X-ray tomography. M.G. did the X-ray tomography image analysis and visualization. B.X. contributed to the mineral's species consulting and X-ray diffraction experiment. S.G. contributed to the cone calorimeter measurement, LOI and assessment of their data. I.B. contributed to conceiving and designing the study and to the drafting of the manuscript. All authors contributed to the manuscript and have given final approval for publication.

Supporting Information: The Supporting Information is available free of charge on the ACS Publications website. It contains:

Section 1: Materials and methods

Section 2: Chemical equations

Section 3: Figure S1 to S9

Section 4: Modeling of the combustion process

Section 5: Supplementary movie captions

Section 6: Reference

REFERENCES

(1) Frey, M.; Widner, D.; Segmehl, J. S.; Casdorff, K.; Keplinger, T.; Burgert, I. Delignified and Densified Cellulose Bulk Materials with Excellent Tensile Properties for Sustainable Engineering. *ACS Appl. Mater. Interfaces* **2018,** *10*, 5030-5037.

(2) Song, J.; Chen, C.; Zhu, S.; Zhu, M.; Dai, J.; Ray, U.; Li, Y.; Kuang, Y.; Li, Y.; Quispe, N.; Yao, Y.; Gong, A.; Leiste, U. H.; Bruck, H. A.; Zhu, J. Y.; Vellore, A.; Li, H.; Minus, M. L.; Jia, Z.; Martini, A.; Li, T.; Hu, L. Processing Bulk Natural Wood into A High-Performance Structural Material. *Nature* **2018,** *554*, 224-228.

(3) Okahisa, Y.; Yoshida, A.; Miyaguchi, S.; Yano, H. Optically Transparent Wood–Cellulose Nanocomposite as A Base Substrate for Flexible Organic Light-Emitting Diode Displays. *Compos. Sci. Technol.* **2009,** *69*, 1958-1961.

(4) Nogi, M.; Iwamoto, S.; Nakagaito, A. N.; Yano, H. Optically Transparent Nanofiber Paper. *Adv. Mater.* **2009,** *21*, 1595-1598.

(5) Li, Y.; Fu, Q.; Yu, S.; Yan, M.; Berglund, L. Optically Transparent Wood from a Nanoporous Cellulosic Template: Combining Functional and Structural Performance. *Biomacromolecules* **2016,** *17*, 1358-1364.

(6) Zhu, M.; Song, J.; Li, T.; Gong, A.; Wang, Y.; Dai, J.; Yao, Y.; Luo, W.; Henderson, D.; Hu, L. Highly Anisotropic, Highly Transparent Wood Composites. *Adv. Mater.* **2016,** *28*, 5181-5187.

(7) Merk, V.; Chanana, M.; Gierlinger, N.; Hirt, A. M.; Burgert, I. Hybrid Wood Materials with Magnetic

Anisotropy Dictated by the Hierarchical Cell Structure. *ACS Appl. Mater. Interfaces* **2014,** *6*, 9760-9767.

(8) Hale, R. C.; La Guardia, M. J.; Harvey, E. P.; Gaylor, M. O.; Mainor, T. M.; Duff, W. H. Persistent Pollutants in Land-Applied Sludges. *Nature* **2001,** *412*, 140-141.

(9) Shaw, S. Halogenated Flame Retardants: Do The Fire Safety Benefits Justify the Risks? *Rev. Environ. Health* **2010,** *25* (4), 261-306.

(10) Li, Y.-C.; Schulz, J.; Mannen, S.; Delhom, C.; Condon, B.; Chang, S.; Zammarano, M.; Grunlan, J. C. Flame Retardant Behavior of Polyelectrolyte−Clay Thin Film Assemblies on Cotton Fabric. *ACS Nano* **2010,** *4*, 3325-3337.

(11) Liu, A.; Walther, A.; Ikkala, O.; Belova, L.; Berglund, L. A. Clay Nanopaper with Tough Cellulose Nanofiber Matrix for Fire Retardancy and Gas Barrier Functions. *Biomacromolecules* **2011,** *12*, 633-641.

(12) Carosio, F.; Kochumalayil, J.; Cuttica, F.; Camino, G.; Berglund, L. Oriented Clay Nanopaper from Biobased Components—Mechanisms for Superior Fire Protection Properties. *ACS Appl. Mater. Interfaces* **2015,** *7*, 5847-5856.

(13) Higginbotham, A. L.; Lomeda, J. R.; Morgan, A. B.; Tour, J. M. Graphite Oxide Flame-Retardant Polymer Nanocomposites. *ACS Appl. Mater. Interfaces* **2009,** *1*, 2256-2261.

(14) Kashiwagi, T.; Du, F.; Douglas, J. F.; Winey, K. I.; Harris Jr, R. H.; Shields, J. R. Nanoparticle Networks Reduce the Flammability of Polymer Nanocomposites. *Nat. Mater.* **2005,** *4*, 928-933.

(15) Ming, P.; Song, Z.; Gong, S.; Zhang, Y.; Duan, J.; Zhang, Q.; Jiang, L.; Cheng, Q. Nacre-Inspired Integrated Nanocomposites with Fire Retardant Properties by Graphene Oxide and Montmorillonite. *J. Mater. Chem. A* **2015,** *3*, 21194-21200.

(16) Thirumal, M.; Singha, N. K.; Khastgir, D.; Manjunath, B. S.; Naik, Y. P. Halogen-Free Flame-Retardant Rigid Polyurethane Foams: Effect of Alumina Trihydrate and Triphenylphosphate on the Properties of Polyurethane Foams. *J. Appl. Polym. Sci.* **2010,** *116*, 2260-2268.

(17) Finnemore, A.; Cunha, P.; Shean, T.; Vignolini, S.; Guldin, S.; Oyen, M.; Steiner, U. Biomimetic Layer-by-Layer Assembly of Artificial Nacre. *Nat. Commun.* **2012,** *3*, 966.

(18) Mao, L.-B.; Gao, H.-L.; Yao, H.-B.; Liu, L.; Cölfen, H.; Liu, G.; Chen, S.-M.; Li, S.-K.; Yan, Y.-X.;

Liu, Y.-Y.; Yu, S.-H. Synthetic Nacre by Predesigned Matrix-Directed Mineralization. *Science* **2016,** *354*, 107-110.

(19) Wang, Y.; Azaïs, T.; Robin, M.; Vallée, A.; Catania, C.; Legriel, P.; Pehau-Arnaudet, G.; Babonneau, F.; Giraud-Guille, M.-M.; Nassif, N. The Predominant Role of Collagen in the Nucleation, Growth, Structure and Orientation of Bone Apatite. *Nat. Mater.* **2012,** *11*, 724-733.

(20) Wegst, U. G. K.; Bai, H.; Saiz, E.; Tomsia, A. P.; Ritchie, R. O. Bioinspired Structural Materials. *Nat. Mater.* **2014,** *14*, 23-36.

(21) Merk, V.; Chanana, M.; Keplinger, T.; Gaan, S.; Burgert, I. Hybrid Wood Materials with Improved Fire Retardance by Bio-Inspired Mineralisation on the Nano- and Submicron Level. *Green Chem.* **2015,** *17*, 1423-1428.

(22) Merk, V.; Chanana, M.; Gaan, S.; Burgert, I., Mineralization of Wood by Calcium Carbonate Insertion for Improved Flame Retardancy. *Holzforschung*, **2016,** 70, 867-876.

(23) Robertson, W. G.; Jones, J. S.; Heaton, M. A.; Stevenson, A. E.; Markwell, P. J. Predicting the Crystallization Potential of Urine from Cats and Dogs with Respect to Calcium Oxalate and Magnesium Ammonium Phosphate (Struvite). *J. Nutr.* **2002,** *132*, 1637S-1641S.

(24) Yetilmezsoy, K.; Kocak, E.; Akbin, H. M.; Özçimen, D. Utilization of Struvite Recovered from High-Strength Ammonium-Containing Simulated Wastewater as Slow-Release Fertilizer and Fire-Retardant Barrier. *Environ. Technol.* **2018**, 1-18.

(25) Hanagasaki, H. Fireproofing of Wood Materials and Fire-Resistant Wood Materials. JP2012121274A, 2012.

(26) Lowden, L. A.; Hull, T. R. Flammability Behaviour of Wood and a Review of the Methods for Its Reduction. *Fire Sci. Rev.* **2013,** *2*, 4.

(27) Doyle, J. D.; Parsons, S. A. Struvite Formation, Control and Recovery. *Water Res.* **2002,** *36*, 3925-3940.

(28) Schartel, B.; Hull, T. R. Development of Fire-Retarded Materials—Interpretation of Cone Calorimeter Data. *Fire and Mater.* **2007,** *31*, 327-354.

(29) Gao, M.; Sun, C. Y.; Wang, C. X. Thermaldegradation of Wood Treated with Flame Retardants. *J. Therm. Anal. Calorim.* **2006,** *85*, 765-769.

(30) Byrne, C. E.; Nagle, D. C. Carbonization of Wood for Advanced Materials Applications. *Carbon* **1997,** *35*, 259-266.

(31) Braun, U.; Balabanovich, A. I.; Schartel, B.; Knoll, U.; Artner, J.; Ciesielski, M.; Döring, M.; Perez, R.; Sandler, J. K. W.; Altstädt, V.; Hoffmann, T.; Pospiech, D. Influence of the Oxidation State of Phosphorus on the Decomposition and Fire Behaviour of Flame-Retarded Epoxy Resin Composites. *Polymer* **2006,** *47*, 8495-8508.

(32) Schartel, B. Phosphorus-based Flame Retardancy Mechanisms—Old Hat or a Starting Point for Future Development? *Materials* **2010,** *3*, 4710-4745.

(33) Levchik, S. V.; Weil, E. D. A Review of Recent Progress in Phosphorus-Based Flame Retardants. *J. Fire Sci.* **2006,** *24*, 345-364.

(34) Wolf-Gladrow, D. A Lattice Boltzmann Equation for Diffusion. *J. Stat. Phys.* **1995,** *79*, 1023-1032.

(35) Mendoza, M.; Wittel, F. K.; Herrmann, H. J. Simulation of Flow of Mixtures through Anisotropic Porous Media Using a Lattice Boltzmann Model. *Eur. Phys. J. E* **2010,** *32*, 339-348.

(36) Spurr, A. R. A low-viscosity epoxy resin embedding medium for electron microscopy. *J. Ultrastruct. Res.* **1969,** *26*, 31-43.

A fire-retardant hybrid material consisting of renewable wood and the biomineral struvite opens the avenue for sustainable construction.

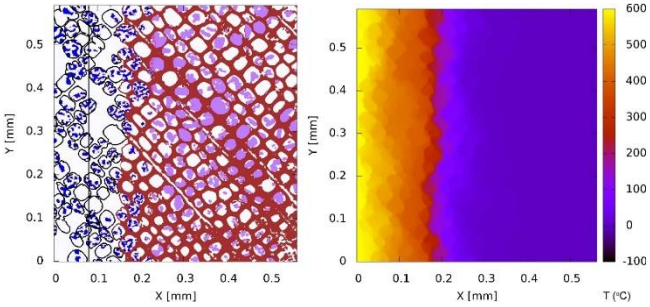

TOC